inorganics

MDPI

Article

Synthesis of High-Crystallinity Mg-Al Hydrotalcite with a Nanoflake Morphology and Its Adsorption Properties for Cu^{2+} from an Aqueous Solution

Nai-Cai Xu [1,2,3,*], Dan-Dan Shi [1], Ying Zhang [1], Kai-Peng Zhong [1,2], Jing Liu [1,2], Qi Zhao [1,2], Qiang Gao [1,2] and Shao-Ju Bian [1,2,3,*]

[1] School of Chemistry and Chemical Engineering, Qinghai Normal University, Xining 810008, China
[2] Qinghai Key Laboratory of Advanced Technology and Application of Environmental Functional Materials, Xining 810016, China
[3] Academy of Plateau Science and Sustainability, People's Government of Qinghai Province & Beijing Normal University, Xining 810016, China
* Correspondence: xunc@qhnu.edu.cn (N.-C.X.); 20201121@qhnu.edu.cn (S.-J.B.); Tel./Fax: +86-971-630-7635 (N.-C.X. & S.-J.B.)

Abstract: A magnesium–aluminum-layered double hydroxide (Mg-Al LDH) with a nano-lamellar morphology was prepared by using a homogeneous precipitation and hydrothermal method, and a calcination product (Mg-Al LDO) of the Mg-Al LDH was also obtained in this work. The XRD, TEM, SEM, FTIR, N_2 ad/desorption, and TG-DTG techniques were employed to characterize the microstructures, morphologies, and thermostability levels of these two materials in detail. The results showed that both the Mg-Al LDH and Mg-Al LDO had mesoporous structures and nanoplate morphologies, with diameters of 50~200 nm. The Mg-Al LDH was transformed into Mg-Al LDO at 773 K in an air atmosphere. The adsorption properties of the Mg-Al LDH were investigated systematically with a copper chloride solution as a simulated waste. The experimental results demonstrated that the pH value of the solution had an obvious influence on its Cu^{2+} adsorption capacity, and the optimal pH value was approximately 5.0. The adsorption kinetics results showed that the Mg-Al LDH had a rapid adsorption rate, and the equilibrium adsorption capacity was 62.11 mg/g. Additionally, the Cu^{2+} adsorption could be commendably described using a pseudo-second-order model, demonstrating that the adsorption behavior is regulated by chemical sorption. The adsorption thermodynamic results indicated that the adsorption process was spontaneous at temperatures above 318 K. Moreover, the ΔG^0 values decreased as the temperature was raised, which indicated that a higher temperature can cause a greater impetus for Cu^{2+}adsorption. In addition, the positive values of the ΔH^0 indicated that the Cu^{2+} adsorption was endothermic, and the positive ΔS^0 values revealed an increase in the confusion at the solid–liquid interface of the adsorbent.

Keywords: Mg-Al LDH; lamellar morphology; Cu^{2+}; adsorption; kinetics

Citation: Xu, N.-C.; Shi, D.-D.; Zhang, Y.; Zhong, K.-P.; Liu, J.; Zhao, Q.; Gao, Q.; Bian, S.-J. Synthesis of High-Crystallinity Mg-Al Hydrotalcite with a Nanoflake Morphology and Its Adsorption Properties for Cu^{2+} from an Aqueous Solution. *Inorganics* **2023**, *11*, 369. https://doi.org/10.3390/inorganics11090369

Academic Editors: Richard Dronskowski, Christian Julien, Rainer Niewa, Guido Kickelbick, Alexander S. Novikov, Gary Hix and Hans-Conrad zur Loye

Received: 26 July 2023
Revised: 1 September 2023
Accepted: 8 September 2023
Published: 15 September 2023

1. Introduction

With the development of social economies and industrial development, toxic heavy metal contamination in various types of water is becoming more and more serious, and it has become a serious threat to human and environmental health [1,2]. It has become one of the most important environmental problems from an ecological and health perspective. Heavy metals are highly toxic and have long-term sustainability, and they will not degrade by themselves in the environment but can only migrate and transform to other substances [3–6]. Additionally, some heavy metals may combine with organic matter to convert into more toxic organometallic compounds [7]. The accumulation of heavy metals through the biological chain will eventually enter the human body and cause serious harm to human health, even leading to death when its concentration reaches a certain degree.

There are many treatment methods for heavy metal ions in wastewater according to reports in the literature. These mainly include chemical precipitation [8], chemical reduction [9], ion exchange [10], membrane separation [11], adsorption [12], and biological flocculation [13]. Among these, the adsorption method is a type of wastewater treatment technology with high efficiency, a low cost, and wide application. Therefore, the development of efficient, cheap, and reproducible adsorbents has always been a main research hotspot in this field. The commonly used sorbents for the removal of heavy metal ions from aqueous solutions are fertilizer industry waste [14], polymers [15], modified chitosans [16], iron oxides [17], Mg-Al LDHs [18], activated alumina [19], and charcoal [20]. Among these adsorbents, LDHs and their derivates have attracted great attention due to being inexpensive, having a large adsorption capacity, and possessing special pore structure properties [21].

Hydrotalcite materials have excellent ion exchange and adsorption properties due to their special sandwich structure, along with the controllability of their layer intervals and anionic exchange capabilities and their high specific surface areas and adequate channel structures [22]. Meanwhile, LDHs have ample hydroxyl functional groups and super-large surface areas for effectively eliminating heavy metals from aqueous solutions. For example, Tran et al. [23] prepared a Mg-Al LDH that was intercalated with the organic acid anions of citrate and malate for the effective removal of Pb^{2+} and Cu^{2+} from an aqueous solution. Huang et al. [24] investigated Cr(VI) removal using a biochar embellished with a Mg-Al LDH inserted with ethylenediaminetetraacetic acid. Soltani et al. [25] prepared a hierarchic LDH/MOF nanomaterial as a prospective adsorbent for the concurrent elimination of toxic dyes and inorganic heavy metal ions from wastewater. In terms of the material structure, the higher the degree of crystallinity, the more stable the properties of the substance, and the better the physical and chemical properties in general. So increasing the degree of crystallinity can make the physical and chemical properties of a substance more stable [26,27]. However, according to the literature, the crystallinity of most Mg-Al LDHs is not very high [28,29], which has an adverse effect on the mechanical properties and stability of the material. In particular, contact in the solid–liquid phase interface in a solution will weaken the stability of a material, to a certain extent.

In order to further improve the crystallinity of a Mg-Al LDH and perfect its physical and chemical properties, we combined homogeneous precipitation and hydrothermal technology to prepare a Mg-Al LDH material with a high degree of crystallinity in this work. XRD, SEM, TEM, N_2 ad/desorption, FTIR, and TG-DTG technologies were used to systematically characterize the microarchitectures, morphologies, and thermostability levels of the Mg-Al LDH. In addition, the adsorption properties of Cu^{2+} from an aqueous solution were investigated by using the solution's pH, adsorption kinetics, thermodynamics, and dose adsorption experiments.

2. Materials and Methods

2.1. Materials

The experimental water was deionized water. $CuCl_2{\cdot}2H_2O$ was dissolved into the deionized water to prepare Cu^{2+} stock solutions of different concentrations. Magnesium chloride ($MgCl_2{\cdot}6H_2O$), sodium hydroxide (NaOH), sodium carbonate (Na_2CO_3), aluminum nitrate ($Al(NO_3)_3{\cdot}9H_2O$), copper chloride ($CuCl_2{\cdot}2H_2O$), and hydrochloric acid (HCl) were obtained from the Shanghai McLean Chemical Reagent Company Limited, and all of them were analytical-grade reagents.

2.2. Adsorbent Preparation

Certain amounts of $MgCl_2{\cdot}6H_2O$ and $Al(NO_3)_3{\cdot}9H_2O$ were dissolved in 80 mL of deionized water to obtain a mixture which was denoted as solution A. Then, 6.4 g of NaOH and 4.24 g of Na_2CO_3 were diluted into 80 mL deionized water, successively, to obtain solution B. Solutions A and B were stirred separately for a period of time, and then solution A was added to solution B, drop by drop, to obtain a uniform reaction system that was

stirred persistently. After dripping, the solution pH values were controlled between 9 and 10, and then the reactant continued to be fully stirred for another 30 min. Then, the mixture was shifted into a Teflon-lined stainless-steel vessel after being stirred constantly, and it was autoclaved at 393 K for 24 h. After cooling to room temperature, the mixture was filtered, washed alternately with deionized water and absolute ethyl alcohol to become neutral, and dried in an oven at 338 K for 12 h to obtain a white sample which was denoted as Mg-Al LDH. A certain number of synthesized Mg-Al LDH samples were roasted in a muffle furnace at 726 K for 4 h to obtain a white powdery substance which was denoted as Mg-Al LDO.

2.3. Adsorption Experiment Method

The working Cu^{2+} solution of 100 mg/L was prepared by dissolving a certain amount of $CuCl_2 \cdot 2H_2O$ into deionized water and reserving it in a 1000 mL measuring flask.

To detect the influence of solution pH value on Cu^{2+} adsorption, 50 mL of 100 mg/L Cu^{2+} was mingled with 50 mg of Mg-Al LDH in a 100 mL polyethylene bottle that was closed tightly and placed in a self-shaking shaker under vibration at 298 K for 6 h. The solution pH values were controlled by using 0.1 mol/L of NaOH or 0.1 mol/L of HCl, and the pH value was surveyed by a pH meter.

For the adsorption kinetic test, 50 mg of synthesized Mg-Al LDH adsorbent was added to 50 mL of 100 mg/L Cu^{2+} solution (the pH value was not adjusted) under stirring at 298 K for 5, 10, 20, 30, 60, 90, 120, 180, 240, and 360 min, respectively. Then, the same volume of suspension was taken out at each time interval and immediately centrifuged at 8000 rpm to isolate the solution from the mixture. The residual Cu^{2+} concentration in the aqueous solution was measured using an atomic absorption spectrophotometer.

To explore the influence of temperature on Cu^{2+} adsorption, 50 mL of 100 mg/L Cu^{2+} (the solution pH was not adjusted) was mingled with 50 mg of Mg-Al LDH in a polyethylene bottle that was closed tightly and placed in a self-shaking shaker at 298 K, 308 K, and 318 K, respectively.

In the experiments that investigated the effect of dose on adsorption performance, 50 mL of 100 mg/L Cu^{2+} (the solution pH was not adjusted) was mixed with different-quality Mg-Al LDH samples in polyethylene bottles that were closed tightly and placed in a self-shaking shaker at 298 K for 6 h.

After the adsorption experiments were finished, the mixtures were percolated and the concentrations of Cu^{2+} were analyzed by an atomic absorption spectrophotometer. The adsorption capacities (q_e, mg/g) and removal rates (η%) were calculated using the following two formulas, respectively:

$$q_e = \frac{(c_0 - c_e)}{m} \times V \text{ and} \quad (1)$$

$$\eta = \frac{(c_0 - c_e)}{c_0} \times 100 \quad (2)$$

In the above formulas, q_e (mg/g) is the Cu^{2+} adsorption capacity, c_0 and c_e are the original and equilibrium concentrations of Cu^{2+} (mg/L), V (L) is the solution volume, and m (g) is the adsorbents mass.

2.4. Analytical and Characterization Methods

X-ray diffraction (XRD) diagrams of the products were tested on an X'pert Pro X-ray diffractometer (Philips, Eindhoven, The Netherlands) to determine their crystal structures. Scanning electron microscopy (SEM) experiments were conducted on a JSM-5610LV/INCA electron microscope (JEOL, Tokyo, Japan). Transmission electron microscope (TEM) images were acquired using a JEM-2100 microscope (JEOL, Japan) that was handled at 200 kV. In order to clearly define the pore geometries and pore diameters, the Mg-Al hydrotalcite samples were measured via N_2-sorption, and a BJH analysis of the individual desorption

isotherm experiments was conducted. Brunauer–Emmett–Teller (BET) specific surface areas were obtained from the adsorption information in the relative pressures between 0.05 and 0.30, and the pore diameters were determined using the Barrett–Joyner–Halenda (BJH) model while the total pore volumes were determined from the amount adsorbed at a relative pressure of 0.995. The pore geometries, such as "ink bottle", "slit-like", and "cylindrical" shapes, were obtained according to the types of adsorption and desorption isotherms and the hysteresis loops. Nitrogen ad/desorption was performed on Quantachrome Autosorb-iQ equipment (Quantachrome, Boynton Beach, FL, USA) at −469 K. Fourier-transform infrared spectroscopy (FTIR) spectra of the samples were obtained by using a spectrometer (NICOLET Nexus 470, Nicolet, Ramsey, MN, USA) and effecting limits of 4000~400 cm^{-1} with the specimens prepared by the KBr method. The TG-DTG experiment was carried out on a PerkinElmer STA6000 instrument in dry-air ambience with a 10 °C/min heating rate. The concentrations of Cu^{2+} were determined by an atomic absorption spectrophotometer (TAS-990, Puyang general, Beijing, China).

3. Results and Discussion

3.1. Sample Characterization

The XRD patterns of the Mg-Al LDH and Mg-Al LDO are shown in Figure 1. It can be observed in Figure 1a that the Mg-Al LDH showed sharp and symmetric diffraction peaks at 2θ of 11.6°, 23.42°, and 34.84°, which corresponded to the (003), (006), and (009) crystal faces of the hydrotalcite (JCPDS 98-000-6296), suggesting that hydrotalcite characteristics with a layered structure and a high degree of crystallinity were obtained [30]. In addition, it can be clearly seen in Figure 1b that the characteristic diffraction peaks ((003) and (006)) of the Mg-Al LDH disappeared after high-temperature calcination, indicating that the structure of the Mg-Al LDH was totally damaged, and there was chaos in the residual layers [31]. Moreover, the image shows that the calcined products of the Mg-Al LDH were referred to as Mg-Al LDO while the outcome of the wide peaks was attributed to the generation of periclase [31].

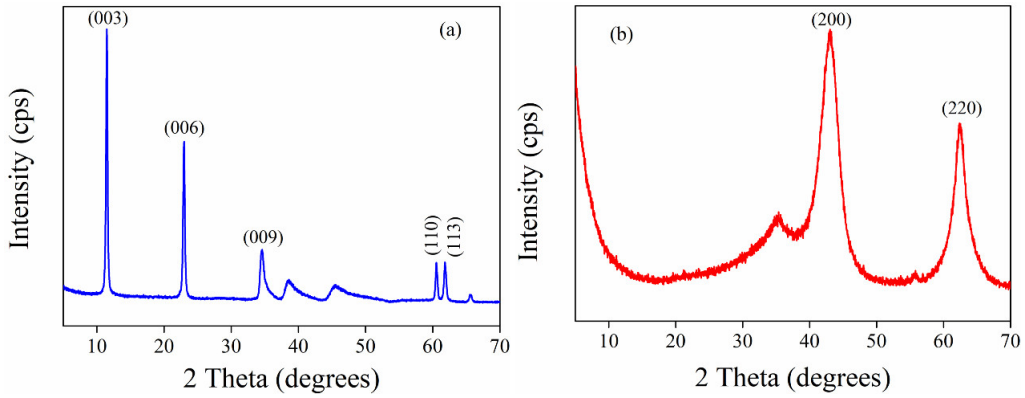

Figure 1. The XRD patterns of the (**a**) Mg-Al LDH and (**b**) Mg-Al LDO.

The micromorphologies and dispersion characteristics of the Mg-Al LDH and Mg-Al LDO are shown in Figure 2. It can be seen in Figure 2a–c that the synthesized Mg-Al LDH had a typical lamellar structure [32]. However, the lamellar sizes and thicknesses were different and the overlap phenomenon between the sheets was prominent. In addition, the degree of dispersion of the samples was not uniform, indicating the samples had high surface energy levels. Figure 2d–f shows the morphology characteristics of the Mg-Al LDO. It can be seen that the shape of the Mg-Al LDO was also that of a laminar microstructure, with a uniform size. The results showed that the morphologies of the synthesized samples did not change significantly after calcination.

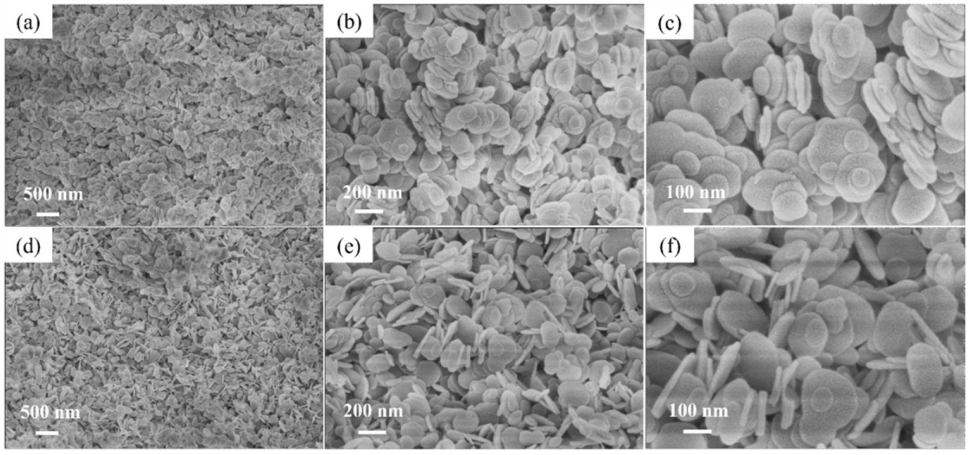

Figure 2. SEM images of (**a**–**c**) the Mg-Al LDH and (**d**–**f**) Mg-Al LDO.

Figure 3 shows the TEM images of the Mg-Al LDH and Mg-Al LDO samples. It can be observed in Figure 3a that the morphology of the Mg-Al LDH, with diameters ranging from tens to hundreds of nanometers, was mainly lamellar, which was consistent with the typical plate morphology of hydrotalcite [33]. In addition, a small number of rod-like substances also appeared in the Mg-Al LDH product, and the reason for this phenomenon was that some individual rod-like morphologies were not completely transformed to lamellar structures during the reaction process (Figure 3b). Figure 3c shows a complete lattice fringe, corresponding to the high-resolution transmission electron microscope image of the Mg-Al LDH, which indicated that the crystal growth was relatively orderly. Figure 3e,f shows the transmission electron microscopy images of the Mg-Al LDO. It can be observed that the morphology of the Mg-Al LDO was basically the same as that of the Mg-Al LDH. The images show a nanoplate morphology with a certain degree of agglomeration, which indicated that the surface energy of the sample was relatively high.

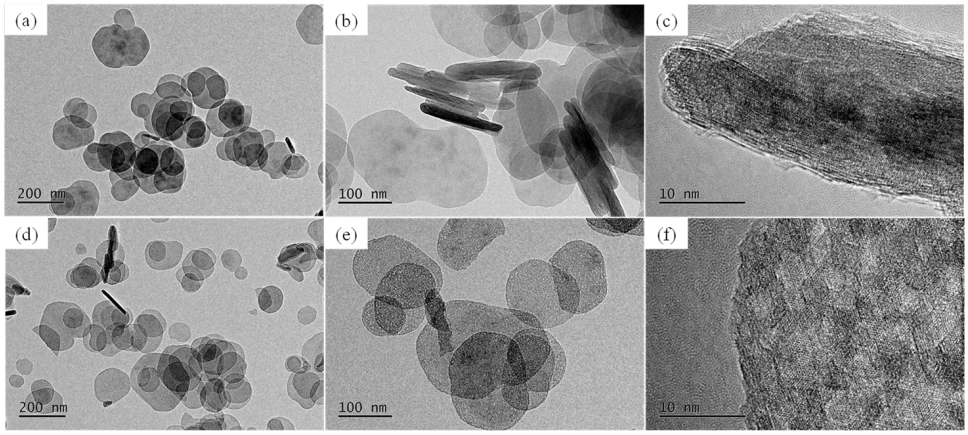

Figure 3. TEM images of the (**a**–**c**) Mg-Al LDH and (**d**–**f**) Mg-Al LDO.

Figure 4 shows the N_2 ad/desorption isotherms and the pore-size distribution curves of the Mg-Al LDH and Mg-Al LDO nanomaterials. It can be seen in the curve features in Figure 4a that both the Mg-Al LDH and Mg-Al LDO were type IV isotherms with H3 shape hysteresis loops according to the IUPAC classification [34,35], indicating the existence of mesoporosity and slit-like shapes in the two samples. The pore-size distribution curves of the samples are plotted in Figure 4b. It can be observed that a majority of the pore sizes were found to be in the range of 0~30 nm, suggesting that a large degree of mesoporosity existed in both the Mg-Al LDH and Mg-Al LDO materials. In addition, the pore volume change rate of the Mg-Al LDH at 63.03 nm was the largest, and that of the Mg-Al LDO, at

42.25 nm, was larger. These results showed that the number of pores with pore sizes ranging from 25 nm to 70 nm was reduced after the Mg-Al LDH calcination. As summarized in Table 1, the BET specific surface areas of the Mg-Al LDH and Mg-Al LDO were 50.21 and 115.71 m^2/g, respectively. The pore volumes of the Mg-Al LDH and Mg-Al LDO were 0.39 and 0.31 cm^3/g, respectively. In comparing the Mg-Al-LDO samples after calcination to the Mg-Al-LDH nanosheets, it was obvious that the BET surface areas of the Mg-Al LDO were significantly increased. However, the pore volumes decreased slightly. This may have been because the pore structures of the Mg-Al LDH collapsed during calcination, thus reducing the pore volumes of the material, and at this time, more nanoparticles were obtained, which increased the specific surface areas of the nanomaterials. The result showed that more pores were formed in the Mg-Al LDO, which resulted in a large increase in its specific surface area.

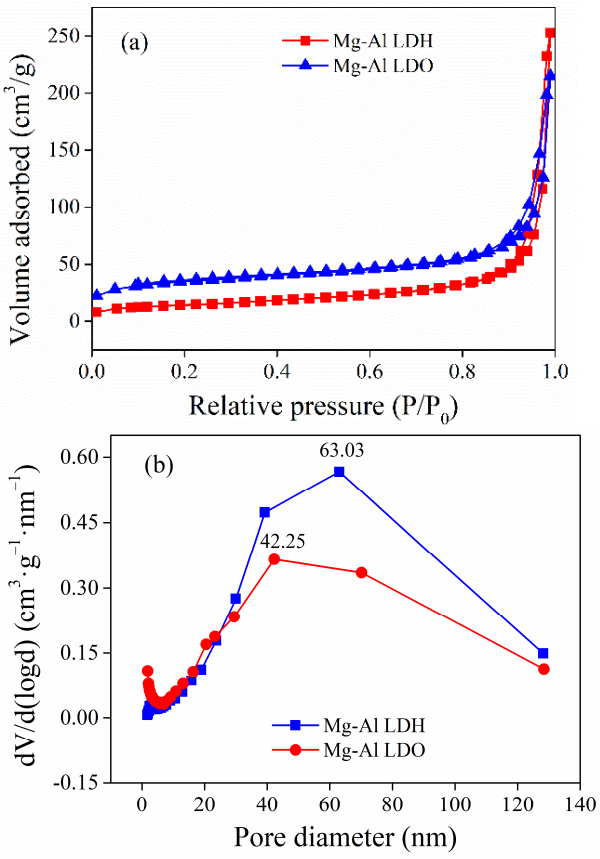

Figure 4. Nitrogen ad/desorption isotherms (**a**) and pore-size distribution curves (**b**) of the Mg-Al LDH and Mg-Al LDO.

Table 1. Structural property parameters of the Mg-Al LDH and Mg-Al LDO samples.

Parameters	Mg-Al LDH	Mg-Al LDO
BET surface area (m^2/g)	50.21	115.71
Pore volume (cm^3/g)	0.39	0.31
Average pore diameter (nm)	63.03	42.25

The FTIR spectra of the Mg-Al LDH and Mg-Al LDO are shown in Figure 5. It can be seen in Figure 5a that there were stretching vibration peaks of the H_2O and –OH groups near 3543 cm^{-1} and there were bending vibration peaks of the H_2O and –OH groups near 1642 cm^{-1}, indicating that there were water molecules and hydroxyl groups in the spaces between the hydrohalic-like layers [36]. The absorption peaks can be obviously seen at 1377 cm^{-1} in the spectrum of the Mg-Al LDH, which agreed with the vibrational

modes of the CO_3^{2-} anions [37]. In addition, in the spectrum of the Mg-Al LDH, the bands at approximately 667 cm^{-1} and 428 cm^{-1} could be assigned to the existence of the lattice translational modes (667 cm^{-1}) and the Al–O bond (428 cm^{-1}) [38,39]. These results confirmed that some functional groups, such as CO_3^{2-}, Al–O, and –OH, were contained in the Mg-Al LDH. It can be seen in Figure 5b that the absorption peaks of the Mg-Al LDO were very similar to those of the Mg-Al LDH.

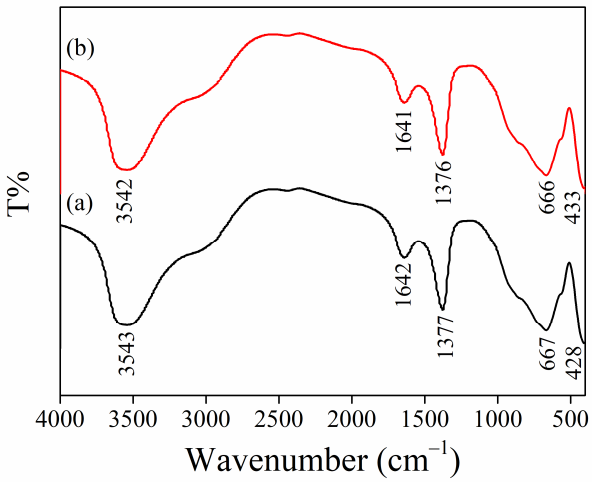

Figure 5. FTIR spectra of the (**a**) Mg-Al LDH and (**b**) Mg-Al LDO.

The TG and DTG curves of the Mg-Al LDH are shown in Figure 6. As presented, there were two weightlessness stages for the Mg-Al LDH in the continuous heating process. The first stage of weightlessness from 298 K to 518 K corresponded to the removal of the waters that were physiosorbed on the outside surface of the hydrohalic material and the waters that were intercalated into the interlayer galleries of the Mg-Al LDH [40]. The weight damage of the hydrone for the Mg-Al LDH was 13.75%, indicating the Mg-Al LDH contained a large number of water molecules. The second stage of weightlessness from 518 K to 1073 K was ascribed to the dihydroxylation of the layers and the elimination of the volatile matter arising from the interlayer CO_3^{2-} for the Mg-Al LDH, with a weight loss of 28.15%. The great weight damage in the second stage demonstrated that there were many OH^- groups on the surface and with CO_3^{2-} in the interlayers of the Mg-Al LDH [41]. Moreover, it can be noticed from the DTG curve that there was an obvious endothermic peak at approximately 483 K which was associated with the loss of the exposed OH^- present on the external surfaces of the Mg-Al LDH. In addition, there was an obvious endothermic peak at 673 K which was assumed to be due to dihydroxylation and decarbonation [22].

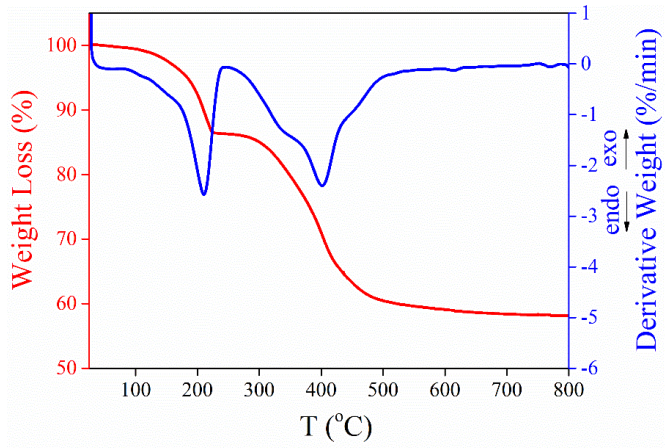

Figure 6. TG and DTG curves of the Mg-Al LDH adsorbent.

3.2. Batch Adsorption of Cu^{2+} onto the Mg-Al LDH

3.2.1. The Effect of Solution pH on Cu^{2+} Adsorption

Solution pH value has a significant influence on adsorption performance in the adsorption process because the charge and adsorption active sites on the surfaces of a sorbent and an adsorbate are importantly affected by it [42]. Figure 7 shows the relationship between the original pH value and the Cu^{2+} adsorption capacity. It can be observed that the Cu^{2+}adsorption capacity increased first and then decreased with increasing the pH value from 4 to 9. In particular, the maximum adsorption capacity was 89.13 mg/g when the pH value was approximately 5. This was because the different charge properties of the Mg-Al LDH reacted to the different pH-value environments. The results showed that there were more negative charges on the adsorbent surface. In addition, the Mg-Al LDH would dissolve, to a certain extent, in the strong acidic medium, resulting in the collapse of the layered structures. However, the Cu^{2+} was easily combined with the OH^- ions to precipitate copper hydroxide in the strong alkaline environment, which weakened the process of the adsorption of Cu^{2+} on to the Mg-Al LDH. In view of the related references and our experimental results [43,44], it was known that the optimal pH condition for Cu^{2+}adsorption onto the Mg-Al LDH was a weakly acidic environment. According to the above results, we did not specifically regulate the pH value of the copper chloride solution in the following adsorption experiments because the pH value of the deionized water was approximately 6.

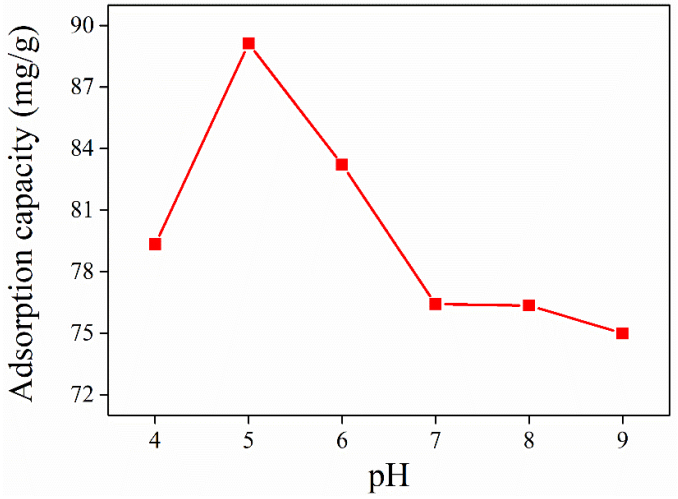

Figure 7. The effect of the solution pH value on Cu^{2+} adsorption onto the Mg-Al LDH (m = 0.05 g, c_0 = 100 mg·L^{-1}, V = 50 mL, T = 298 K, and r = 160 rpm).

3.2.2. Adsorption Kinetics

In order to achieve industrial production, adsorption equilibrium time is an important evaluation index in the wastewater treatment process. The effect of the contact time on Cu^{2+} adsorption onto the Mg-Al LDH was studied at the range of 5~360 min, and the experimental data are presented in Figure 8a. It can be seen that the adsorption rate was fast in the initial stage (5~120 min), and nearly 30% of the Cu^{2+} ions were adsorbed by the Mg-Al LDH in 120 min. Then, with the extension of the contact time, the adsorption capacity of the Cu^{2+} increased little by little until equilibrium was established. When the adsorption time was 360 min, 62.1% of the Cu^{2+} ions were removed. This was mainly due to the abundance of active sites that were absolutely exposed to the Cu^{2+} in the aqueous solution during the initial period, and they were easily taken up. As the adsorption reaction proceeded, the Cu^{2+} adsorbed onto the Mg-Al LDH, which prevented the residual Cu^{2+} from being adsorbed onto the adsorbent due to the electrostatic repulsion between the ions of the same charge. Then, the Cu^{2+} attempted to move into the pores of the Mg-Al LDH, which became difficult. This was a slow and stable process.

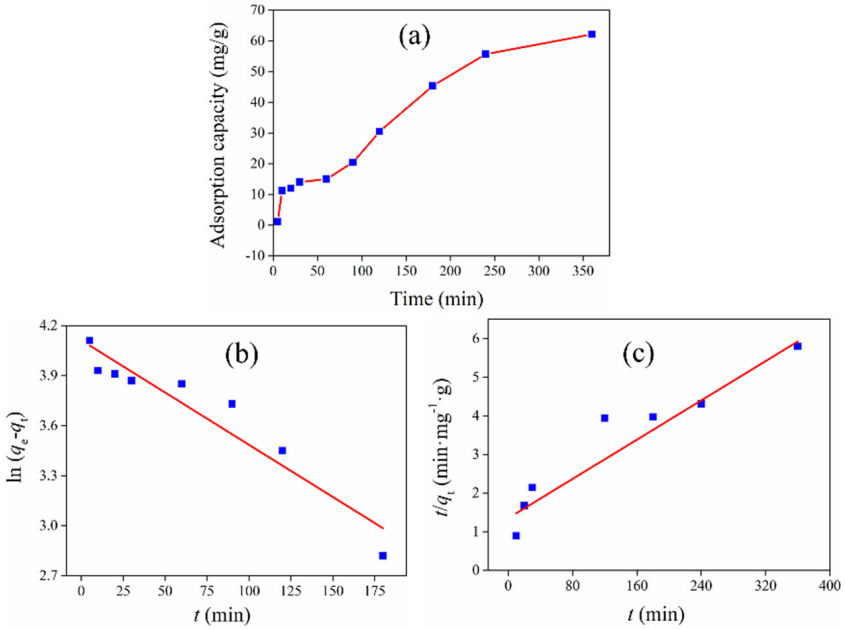

Figure 8. (**a**) The effect of the contact time on the Cu^{2+} adsorption. The adsorption kinetics of Cu^{2+} fitted with a (**b**) pseudo-first-order model and (**c**) a pseudo-second-order model (m = 0.05 g, c_0 = 100 mg·L^{-1}, V = 50 mL, T = 298 K, pH = unregulated, and r = 160 rpm).

In order to further illustrate the adsorption mechanism, pseudo-first-order and pseudo-second-order models [45,46] were adopted to fit the adsorption data. The two equations used were as follows:

$$\ln(q_e - q_t) = \ln q_e - k_1 t \text{ and} \quad (3)$$

$$\frac{t}{q_t} = \frac{1}{k_2 {q_e}^2} + \frac{1}{q_e} t \quad (4)$$

In the above equations, k_1 is the pseudo-first-order adsorption rate constant (min^{-1}), k_2 is the pseudo-second-order adsorption rate constant ($min \cdot g^{-1} \cdot mg^{-1}$), and q_e ($mg \cdot g^{-1}$) and q_t ($mg \cdot g^{-1}$) are the adsorption capacities at an equilibrium state and at any time, respectively.

The fitting results are presented in Figure 8b,c, and the simulation parameters are presented in Table 2. As shown, the correlation coefficient (R^2 = 0.9532) of the pseudo-second-order model was larger than that of the pseudo-first-order model (R^2 = 0.9041). However, the calculated value of q_e obtained by the pseudo-first-order model (67.32 mg/g) was closer to the experimental value of q_e (62.11 mg/g). These results demonstrated that the pseudo-second-order model was more appropriate to fit the adsorption data. Furthermore, the value of k_2 obtained by the pseudo-second-order model was relatively small, suggesting that the adsorption rate decreased with extension of the reaction time. These results demonstrated that the pseudo-second-order model could better simulate the Cu^{2+} adsorption, and it was regulated by the chemical adsorption in the adsorption process [47].

Table 2. Parameters calculated by the pseudo-first-order and pseudo-second-order models.

Experimental		**Pseudo-First-Order**				**Pseudo-Second-Order**				
q_e ($mg \cdot g^{-1}$)	k_1 (min^{-1})	q_e ($mg \cdot g^{-1}$)	R^2	**Standard Error**		k_2 ($g \cdot mg^{-1} \cdot min^{-1}$)	q_e ($mg \cdot g^{-1}$)	R^2	**Standard Error**	
				Intercept	Slope				Intercept	Slope
62.11	0.0084	67.32	0.9041	0.1100	0.00096	0.0001	78.74	0.9532	0.2407	0.0013

3.2.3. The Effect of Dosage on Cu^{2+} Adsorption

The influence of dosage on the adsorption capacity and removal rate of the Mg-Al LDH adsorbent was investigated to determine an optimal solid-to-liquid ratio for the removal of 100 mg/L of Cu^{2+} in an aqueous solution. The mass of the adsorbent varied from 10 mg to 150 mg in 50 mL of Cu^{2+} solution, and the adsorption results are shown in Figure 9. The experimental results showed that the removal percentage of the Cu^{2+} linearly increased when the adsorbent dosage was raised to 90 mg/50 mL. After this adsorption saturation point, the curve no longer rose monotonously, and it gradually showed a stable state. As the dosage of Mg-Al LDH increased from 10 mg to 150 mg, the removal percentage of the Cu^{2+} increased from 30.02% to 66.02%. At the same time, the blue curve shows that the adsorption capacity of the Cu^{2+} showed a monotonically decreasing trend with the increase in the adsorbent mass from 10 mg to 150 mg. This was because the number adsorption sites increased sharply after the addition of adsorbent while the concentration of the Cu^{2+} in the liquid phase decreased when equilibrium was reached with a higher amount of Mg-Al LDH. As the amount of Cu^{2+} in the solid depended on the concentration in the liquid, the Cu^{2+} adsorption capacity also decreased. The results indicated that the optimal solid-to-liquid ratio was 90 mg/50 mL under this adsorption condition.

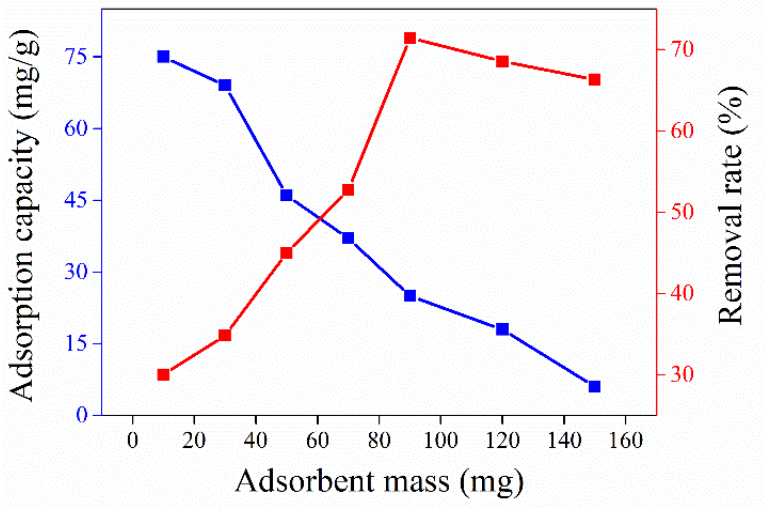

Figure 9. The effect of dosage on the adsorption capacity and removal rate of the Mg-Al LDH (m = 10~150 mg, V = 50 mL, c_0 = 100 mg·L^{-1}, T = 298 K, pH = unregulated, and r = 160 rpm).

3.2.4. Adsorption Thermodynamics

To investigate the influence of temperature on the Cu^{2+} adsorption onto the Mg-Al LDH, the Gibbs free-energy change (ΔG^{θ}), entropy change (ΔS^{θ}), and enthalpy change (ΔH^{θ}) were obtained using the following two formulas [48,49]:

$$\mathrm{Ln}K_L = \frac{\Delta S^{\theta}}{R} - \frac{\Delta H^{\theta}}{RT} \text{ and} \quad (5)$$

$$\Delta G^{\theta} = \Delta H^{\theta} - \mathrm{T}\Delta S^{\theta} \quad (6)$$

In the above formulas, K_L refers to the Langmuir equilibrium constant (L/mol), R refers to the gas molar constant (8.314 J/mol·K), and T refers to the reaction temperature (K). In view of the relationship between ΔG^{θ} and K_L, the values of ΔH^{θ} and ΔS^{θ} were obtained using the intercept and the slope from the Van't Hoff plots of ln K_L versus $1/T$.

It can be seen in Figure 10a that the adsorption capacity of the Mg-Al LDH toward the Cu^{2+} increased with the extension of the reaction temperature, demonstrating that a high temperature was conducive to the diffusion and adsorption of Cu^{2+} onto the Mg-Al LDH.

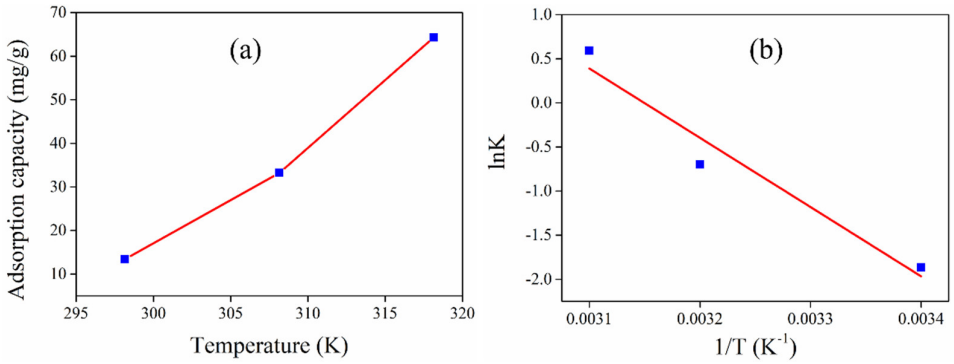

Figure 10. (**a**) The effect of temperature on Cu^{2+} adsorption. (**b**) Van't Hoff plots for the Cu^{2+} adsorption onto the Mg-Al LDH.

The computational thermodynamic parameters are shown in Table 3. As outlined, the ΔG^0 values for the Mg-Al LDH at 298 K and 308 K were positive during the adsorption process, indicating that the Cu^{2+} adsorption onto the Mg-Al LDH was nonspontaneous [28]. However, when the reaction temperature was increased to 318 K, the ΔG^0 values became negative, indicating that the Cu^{2+} adsorption onto the Mg-Al LDH was spontaneous at a higher temperature. Moreover, the ΔG^0 values diminished with increasing reaction temperatures, demonstrating that a higher temperature can produce a greater impetus for Cu^{2+} adsorption. In addition, the positive value of ΔH^0 indicated that the Cu^{2+} adsorption was endothermic, and hyperthermy was beneficial for improving the adsorption performance. Simultaneously, the positive ΔS^0 values disclosed an increase in the disorder at the solid–liquid interface in the solution [50]. During the entire adsorption process, hyperthermia contributed to the Cu^{2+} dissolution and its increased affinity with the Mg-Al LDH, and it was also beneficial for the activation of the active sites on the surface of the adsorbent [51].

Table 3. Values of the thermodynamic parameters for the Cu^{2+} adsorption onto the Mg-Al LDH at various temperatures.

Sample	T (K)	ΔG^{θ} (kJ/mol)	ΔH^{θ} (kJ/mol)	ΔS^{θ} (J/(mol·K)	R^2	Standard Error	
	298	3.97				Intercept	Slope
Mg-Al LDH	308	1.92	65.24	205.49	0.9056	5.6509	1746.40
	318	−0.14					

4. Conclusions

Mg-Al LDH samples with nano-lamellar morphologies and diameters of 50~200 mm were prepared using a homogeneous precipitation and hydrothermal method. Then, the corresponding calcined product, Mg-Al LDO, was also obtained in this work. The characterization results showed that the two samples had similar micro-morphological characteristics, but the latter had a larger BET specific surface area, indicating there were more open-framework structures and reactive sites on the adsorbent's surface. The batch experimental results demonstrated that the Mg-Al LDH, with its nano-lamellar morphology, had a rapid adsorption speed and relatively large adsorption capacity (62.11 mg/g) for Cu^{2+} in a solution. The pH value of the solution had a vital effect on the adsorption efficiency, and the adsorption capacity was the largest when the pH value was approximately 5. The results of the adsorption kinetics indicated that the Cu^{2+} adsorption behavior could be interpreted by a pseudo-second-order model, demonstrating that the adsorption process was controlled by chemical sorption. The results of the dose experiments indicated that the optimal solid-to-liquid ratio was 90 mg/50 mL. The adsorption thermodynamic results indicated that adsorption process was spontaneous at hyperthermia (>318 K), and the ΔG^0 values decreased with increasing temperatures, which indicated that a higher temperature

could produce a greater driving force for Cu^{2+}adsorption onto the Mg-Al LDH in an aqueous solution. These meaningful results could potentially stimulate further study on the synthesis of magnesium aluminum hydrotalcite material and promote its development.

Author Contributions: Conceptualization, N.-C.X. and S.-J.B.; experiment and data processing, Y.Z., J.L., Q.Z. and Q.G.; writing—original draft preparation, N.-C.X., D.-D.S., S.-J.B. and K.-P.Z. All authors have understood and agreed to the published version of this manuscript.

Funding: This research was supported by the key research program for international cooperation in science and technology of Qinghai Province (2023-HZ-811), the "Light of the West" of the Chinese Academy of Sciences and the Qinghai "Kunlun talent" program.

Institutional Review Board Statement: Not applicable.

Informed Consent Statement: Not applicable.

Data Availability Statement: All data and information are included in this paper.

Conflicts of Interest: The authors proclaim no conflicts of interest.

References

1. Lin, G.; Zeng, B.; Li, J.; Wang, Z.-Y.; Wang, S.-X.; Hu, T.; Zhang, L.-B. A systematic review of metal organic frameworks materials for heavy metal removal: Synthesis, applications and mechanism. *Chem. Eng. J.* **2023**, *460*, 141710. [CrossRef]
2. Zheng, L.; Lin, H.; Dong, Y.; Li, B.; Lu, Y. A promising approach for simultaneous removal of ammonia and multiple heavy metals from landfill leachate by carbonate precipitating bacterium. *J. Hazard. Mater.* **2023**, *456*, 131662. [CrossRef]
3. Zhao, K.; Zhao, X.; Gao, T.; Li, X.; Wang, G.; Pan, X.; Wang, J. Dielectrophoresis-assisted removal of Cd and Cu heavy metal ions by using Chlorella microalgae. *Environ. Pollut.* **2023**, *334*, 122110. [CrossRef]
4. Zhao, D.; Peng, Z.; Fang, J.; Fang, Z.; Zhang, J. Programmable and low-cost biohybrid membrane for efficient heavy metal removal from water. *Sep. Purif. Technol.* **2023**, *306*, 122751. [CrossRef]
5. Eibshary, R.; Gouda, A.; Sheikh, R.; Alqahtani, M.; Hanfi, M.; Atia, B.; Sakr, A.; Gado, M. Recovery of W(VI) from wolframite ore using new synthetic chiff base derivative. *Int. J. Mol. Sci.* **2023**, *24*, 7423. [CrossRef] [PubMed]
6. Chang, X.; Yan, J.; Ding, X.; Jia, Y.; Li, S.; Zhang, M. One-dimensional CoMoP nanostructures as bifunctional electrodes for overall water splitting. *Nanomaterials* **2022**, *12*, 3866. [CrossRef] [PubMed]
7. Tripathi, S.; Sharma, P.; Singh, K.; Purchase, D.; Chandra, R. Translocation of heavy metals in medicinally important herbal plants growing on complex organometallic sludge of sugarcane molasses-based distillery waste. *Environ. Technol. Innov.* **2021**, *22*, 101434. [CrossRef]
8. Chen, Q.; Yao, Y.; Li, X.; Lu, J.; Zhou, J.; Huang, Z. Comparison of heavy metal removals from aqueous solutions by chemical precipitation and characteristics of precipitates. *J. Water Process Eng.* **2018**, *26*, 289–300. [CrossRef]
9. Li, K.; Wang, C.; Hu, H.; Zhang, Q. Selective removal of copper from heavy-metals-containing acidic solution by a mechanochemical reduction with zero-valent silicon. *Chem. Eng. J.* **2023**, *466*, 143246. [CrossRef]
10. Fu, Z.-J.; Jiang, S.-K.; Chao, X.-Y.; Zhang, C.-X.; Shi, Q.; Wang, Z.-Y.; Liu, M.-L.; Sun, S.-P. Removing miscellaneous heavy metals by all-in-one ion exchange-nanofiltration membrane. *Water Res.* **2022**, *222*, 118888. [CrossRef]
11. Long, X.; Zhao, G.-Q.; Zheng, Y.-J.; Hu, J.; Zuo, Y.; Luo, W.-J.; Jiao, F.-P. A precise pyromellitic acid grafting prepared multifunctional Mxene membranes for efficient oil-in-water emulsion separation and heavy metal ions removal. *Chem. Eng. J.* **2023**, *472*, 144904. [CrossRef]
12. Kushwaha, J.; Singh, R. Cellulose hydrogel and its derivatives: A review of application in heavy metal adsorption. *Inorg. Chem. Commun.* **2023**, *152*, 110721. [CrossRef]
13. Xiao, X.; Sun, Y.; Liu, J.; Zheng, H. Flocculation of heavy metal by functionalized starch-based bioflocculants: Characterization and process evaluation. *Sep. Purif. Technol.* **2021**, *267*, 118628. [CrossRef]
14. Aoun, M.; El Samrani, A.G.; Lartiges, B.S.; Kazpard, V.; Saad, Z. Releases of phosphate fertilizer industry in the surrounding environment: Investigation on heavy metals and polonium-210 in soil. *J. Environ. Sci.* **2010**, *22*, 1387–1397. [CrossRef]
15. Sowmya, P.; Prakash, S.; Joseph, A. Adsorption of heavy metal ions by thiophene containing mesoporous polymers: An experimental and theoretical study. *J. Solid State Chem.* **2023**, *320*, 123836. [CrossRef]
16. Zhou, Y.; Gao, B.; Zimmerman, A.R.; Fang, J.; Sun, Y.; Cao, X. Sorption of heavy metals on chitosan-modified biochars and its biological effects. *Chem. Eng. J.* **2013**, *231*, 512–518. [CrossRef]
17. Kim, C.-Y.; Kim, S.H.; An, H.-R.; Park, J.-I.; Jang, Y.; Seo, J.; Kim, H.; Son, B.; Jeong, Y.; Jeong, B.; et al. Iron oxide incorporated carbide nanofiber composites for removal of organic pollutants and heavy metals from water. *Ceram. Int.* **2023**, *49*, 17984–17992. [CrossRef]
18. Song, W.; Zhang, X.; Zhang, L.; Yu, Z.; Li, X.; Li, Y.; Cui, Y.; Zhao, Y.; Yan, L. Removal of various aqueous heavy metals by polyethylene glycol modified MgAl-LDH: Adsorption mechanisms and vital role of precipitation. *J. Mol. Liq.* **2023**, *375*, 121386. [CrossRef]

19. Sankararamakrishnan, N.; Jaiswal, M.; Verma, N. Composite nanofloral clusters of carbon nanotubes and activated alumina: An efficient sorbent for heavy metal removal. *Chem. Eng. J.* **2014**, *235*, 1–9. [CrossRef]
20. Ramraj, S.M.; Kubaib, A.; Imran, P.M.; Thirupathy, M.K. Utilizing Sida Acuta leaves for low-cost adsorption of chromium (VI) heavy metal with activated charcoal. *J. Hazard. Mater.* **2023**, *11*, 100338. [CrossRef]
21. Yang, Z.-Z.; Wei, J.-J.; Zeng, G.-M.; Zhang, H.-Q.; Tan, X.-F.; Ma, C.; Li, X.-C.; Li, Z.-H.; Zhang, C. A review on strategies to LDH-based materials to improve adsorption capacity and photoreduction efficiency for CO_2. *Coord. Chem. Rev.* **2019**, *386*, 154–182. [CrossRef]
22. Kumar, P.; Gill, K.; Kumar, S.; Ganguly, S.; Jain, S. Magnetic Fe_3O_4 @MgAl–LDH composite grafted with cobalt phthalocyanine as an efficient heterogeneous catalyst for the oxidation of mercaptans. *J. Mol. Catal. A-Chem.* **2019**, *401*, 48–54. [CrossRef]
23. Tran, H.N.; Lin, C.; Woo, S.H.; Chao, H. Efficient removal of copper and lead by Mg/Al layered double hydroxides intercalated with organic acid anions: Adsorption kinetics, isotherms, and thermodynamics. *Appl. Clay Sci.* **2018**, *154*, 17–27. [CrossRef]
24. Huang, D.; Liu, C.; Zhang, C.; Deng, R.; Wang, R.; Xue, W.; Luo, H.; Zeng, G.; Zhang, Q.; Guo, X. Cr(VI) removal from aqueous solution using biochar modified with Mg/Al layered double hydroxide intercalated with ethylenediaminetetraacetic acid. *Bioresour. Technol.* **2019**, *276*, 127–132. [CrossRef]
25. Soltani, R.; Marjani, A.; Shirazian, S. A hierarchical LDH/MOF nanocomposite: Single, simultaneous and consecutive adsorption of a reactive dye and Cr(VI). *Dalton Trans.* **2020**, *49*, 5323–5335. [CrossRef]
26. Liu, H.; Ji, P.; Han, X. Rheological phase synthesis of nanosized α-$LiFeO_2$ with higher crystallinity degree for cathode material of lithium-ion batteries. *Mater. Chem. Phys.* **2016**, *183*, 152–157. [CrossRef]
27. Wang, Z.; Li, Q.; Chen, X.; Zhang, Q.; Wang, K. High crystallinity makes excellent wear resistance in crosslinked UHMWPE. *Polymer* **2023**, *280*, 126059. [CrossRef]
28. Zhang, J.; Wang, X.; Zhan, S.; Li, H.; Ma, C.; Qiu, Z. Synthesis of Mg/Al-LDH nanoflakes decorated magnetic mesoporous MCM-41 and its application in humic acid adsorption. *Microchem. J.* **2021**, *162*, 105839. [CrossRef]
29. Fang, C.; Liu, W.; Dai, Y.; Wang, Z.; Li, Y.; Cai, L.; Liu, B.; Yang, S.; Wang, J.; Ding, X.; et al. Synthesis of a novel hierarchical pillared Sep@Fe_3O_4/ZnAl-LDH composite for effective anionic dyes removal. *Colloid. Surf. A* **2023**, *663*, 130921.
30. Chen, X.; Liu, W.; Luo, L.; Han, Y.; Zhang, H.; Zheng, S.; Zhang, Y.; Li, P. A green desilication method from highly concentrated chromate solutions by Mg-Al-CO_3 LDH. *Sep. Purif. Technol.* **2022**, *286*, 120432. [CrossRef]
31. Zeng, B.; Wang, Q.; Mo, L.; Jin, F.; Zhu, J.; Tang, M. Synthesis of Mg-Al LDH and its calcined form with natural materials for efficient Cr(VI) removal. *J. Environ. Chem. Eng.* **2022**, *10*, 108605. [CrossRef]
32. Jiménez-López, B.A.; Leyva-Ramos, R.; Salazar-Rábago, J.J.; Jacobo-Azuara, A.; Aragón-Piña, A. Adsorption of selenium (iv) oxoanions on calcined layered double hydroxides of Mg-Al-CO_3 from aqueous solution. Effect of calcination and reconstruction of lamellar structure, Environmental Nanotechnology. *Monit. Manag.* **2021**, *16*, 100580. [CrossRef]
33. Liu, S.; Li, M.; Tang, Y.; Wen, X. A novel Fe_3O_4/MgAl-LDH hollow microspheres for effective removal of dyes from wastewater. *J. Alloys Compd.* **2023**, *959*, 170528. [CrossRef]
34. Kruk, M.; Jaroniec, M. Gas adsorption characterization of ordered organic-inorganic nanocomposite materials. *Chem. Mater.* **2001**, *13*, 3169–3183. [CrossRef]
35. Thommes, M.; Kaneko, K.; Neimark, A.-V.; Olivier, F.-R.; Rouquerol, J.; Sing, K.-S.-W. Physisorption of gases, with special reference to the evaluation of surface area and pore size distribution (IUPAC Technical Report). *Pure Appl. Chem.* **2015**, *87*, 1051–1069. [CrossRef]
36. Xiao, L.; Ma, W.; Han, M.; Cheng, Z. The influence of ferric iron in calcined nano-Mg/Al hydrotalcite on adsorption of Cr (VI) from aqueous solution. *J. Hazard. Mater.* **2011**, *186*, 690–698. [CrossRef]
37. Tran, H.-N.; Lin, C.-C.; Chao, H.-P. Amino acids-intercalated Mg/Al layered double hydroxides as dual-electronic adsorbent for effective removal of cationic and oxyanionic metal ions. *Sep. Purif. Technol.* **2018**, *192*, 36–45. [CrossRef]
38. Palmer, S.J.; Frost, R.L.; Nguyen, T. Hydrotalcites and their role in coordination of anions in Bayer liquors: Anion binding in layered double hydroxides. *Coord. Chem. Rev.* **2009**, *253*, 250–267. [CrossRef]
39. Xu, Z.P.; Jin, Y.G.; Li, S.M.; Hao, Z.P.; Lu, G.Q. Surface charging of layered double hydroxides during dynamic interactions of anions at the interfaces. *J. Colloid Interface Sci.* **2008**, *326*, 522–529. [CrossRef]
40. Extremera, R.; Pavlovic, I.; P'erez, M.R.; Barriga, C. Removal of acid orange 10 by calcined Mg/Al layered double hydroxides from water and recovery of the adsorbed dye. *Chem. Eng. J.* **2012**, *213*, 392–400. [CrossRef]
41. Li, B.; Zhang, Y.; Zhou, X.; Liu, Z.; Liu, Q.; Li, X. Different dye removal mechanisms between monodispersed and uniform hexagonal thin plate-like MgAl–CO_3^{2-}-LDH and its calcined product in efficient removal of Congo red from water. *J. Alloys Compd.* **2016**, *673*, 265–271. [CrossRef]
42. Xu, N.; Liu, J.; Han, L.; Feng, B.; Li, Y.; Yang, Y.; Bian, S. Preparation, modification and adsorption properties of spinel-type $H_{1.6}Mn_{1.6}O_4$ lithium-ion sieves with spiny nanotube morphology. *J. Mater. Sci.* **2023**, *58*, 4707–4725. [CrossRef]
43. Rojas, R.; Perez, M.R.; Erro, E.M.; Ortiz, P.I.; Ulibarri, M.A.; Giacomelli, C.E. EDTA modified LDHs as Cu^{2+} scavengers: Removal kinetics and sorbent stability. *J. Colloid Interface Sci.* **2009**, *331*, 425–431. [CrossRef]
44. Zhu, S.; Khan, M.A.; Wang, F.; Bano, Z.; Xia, M. Rapid removal of toxic metals Cu^{2+} and Pb^{2+} by amino trimethylene phosphonic acid intercalated layered double hydroxide: A combined experimental and DFT study. *Chem. Eng. J.* **2020**, *392*, 123711. [CrossRef]

45. Miyake, Y.; Ishida, H.; Tanaka, S.; Kolev, P.S. Theoretical analysis of the pseudo-second order kinetic model of adsorption. Application to the adsorption of Ag (I) to mesoporous silica microspheres functionalized with thiol groups. *Chem. Eng. J.* **2013**, *21*, 350–357. [CrossRef]
46. Ho, Y.S. Review of second-order models for adsorption systems. *J. Hazard. Mater.* **2006**, *136*, 681–689. [CrossRef]
47. Hao, J.; Han, M.; Wang, C.; Meng, X.G. Enhanced removal of arsenite from water by a mesoporous hybrid material-Thiol-functionalized silica coated activated alumina. *Microporous Mesoporous Mater.* **2009**, *124*, 1–7. [CrossRef]
48. Muhire, C.; Zhang, D.; Xu, X. Adsorption of uranium (VI) ions by LDH intercalated with l-methionine in acidic water: Kinetics, thermodynamics and mechanisms. *Results Eng.* **2022**, *16*, 100686. [CrossRef]
49. Yuan, T.; Chen, M.; Sun, X.; Guan, J.; Zhu, F.; Tang, K.; Zhang, Z.; Liu, Q.; Chen, X. Synthesis of camphor sulfonic acid derivatives modified Mg/Al-LDH for efficient separation of propranolol enantiomers. *Appl. Clay Sci.* **2022**, *224*, 106521. [CrossRef]
50. Zubair, M.; Manzar, M.S.; Mu'azu, N.D.; Anil, I.; Blaisi, N.I.; Al-Harthi, M.A. Functionalized MgAl-layered hydroxide intercalated date-palm biochar for Enhanced Uptake of Cationic dye: Kinetics, isotherm and thermodynamic studies. *Appl. Clay Sci.* **2020**, *190*, 105587. [CrossRef]
51. Guo, Y.; Gong, Z.; Li, C.; Gao, B.; Li, P.; Wang, X.; Zhang, B.; Li, X. Efficient removal of uranium (VI) by 3D hierarchical Mg/Fe-LDH supported nanoscale hydroxyapatite: A synthetic experimental and mechanism studies. *Chem. Eng. J.* **2020**, *392*, 123682. [CrossRef]